AIAA'86

AIAA-86-0208

A Multigrid Method for the Navier-Stokes Equations

L. Martinelli, A. Jameson and F. Grasso

Princeton University, Princeton N. J.

AIAA 24th Aerospace Sciences Meeting

January 6-9, 1986/Reno, Nevada

A MULTIGRID METHOD FOR THE NAVIER STOKES EQUATIONS

by

L. Martinelli, A. Jameson, and F. Grasso
Department of Mechanical and Aerospace Engineering
Princeton University
Princeton, New Jersey 08544
U.S.A.

Abstract

A multigrid method for solving the compressible Navier Stokes equations is presented. The dimensionless conservation equations are discretized by a finite volume technique and time integration is performed by using a multistage explicit algorithm. Convergence to a steady state is enhanced by local time stepping, implicit smoothing of the residuals and the use of multiple grids. The method has been implemented in two different ways: firstly a cell centered and secondly a corner point formulation (i.e. the unknown variables are defined either at the center of a computational cell or at its vertices). Computed results are presented for laminar and turbulent two dimensional flows over airfoils.

1. Introduction

During the past few years there has been a growing interest in the numerical solution of the viscous compressible Navier Stokes equation for aerodynamic configurations. Although it is true that the viscous effects are unimportant outside the boundary layer region, the presence of the boundary layer can have a drastic influence on the global pattern of the flow field, especially in the event of separation. In the transonic regime the presence of the boundary layer can cause the location of the shock wave to shift as much as 20% of the chord. The increased capability of the new generation of computers opens up the possibility of solving numerically at least, the Reynold's averaged compressible equation, provided that a satisfactory turbulence model is used for closure.

The considerable attention given to the development of efficient solution techniques for the Euler equations has produced very accurate and robust algorithms. Among them the finite volume approach of Jameson, Schmidt and Turkel [1] which uses a multistage time marching scheme has been successfully applied to compute the inviscid flow field on geometries of increasing complexity. Indeed, solutions for a complete aircraft were recently obtained [2]. Moreover, development of acceleration techniques, such as the multigrid scheme of Jameson [3], have drastically reduced the cost of computing the inviscid flow over simpler 2-D and 3-D configurations.

This impressive series of successes with the Euler equations has stimulated recently, new interest in the application of explicit methods to the solution of the Navier Stokes equations [4,5]. However, as in the case of the better established implicit schemes [6,7], major improvements in accuracy, robustness and efficiency are still needed.

The principal aim of this work is to present and evaluate an efficient explicit method for the solution of 2-D compressible viscous flows. A multigrid method for solving the compressible Navier Stokes has been developed. In our approach the conservation equations are discretized by a finite volume technique by using either a cell centered or a corner point formulation. A multistage scheme is then used to perform time integration and to drive the solution on multiple grids. Computational efficiency is also enhanced by the use of locally varying time steps and implicit smoothing of the residuals.

In the next sections the governing equations are presented and the numerical algorithm is discussed together with the treatment of the boundary conditions. Finally we shall present computed results of laminar and turbulent flows over airfoils.

2. Governing Equations

A dimensionless conservation form of Navier Stokes equations is used with the following definition of the non-dimensional variables

$$(x^*,y^*) = (x/c;\ y/c), \text{ where c is the chord length.}$$

$$t^* = t(p_\infty/\rho_\infty)^{1/2}/c$$

$$\rho^* = \rho/\rho_\infty$$

$$u^* = u/\sqrt{p_\infty/\rho_\infty}$$

$$v^* = v/\sqrt{p_\infty/\rho_\infty}$$

$$E^* = E/(p_\infty/\rho_\infty)$$

$$p^* = p/p_\infty$$

$$\mu^* = \mu/\mu_\infty \quad \sqrt{\gamma}\, M_\infty/Re$$

$$k^* = C_p(\mu^*/Pr).$$

Dropping the * for the sake of brevity, the Navier Stokes equations in two dimensions and cartesian coordinate system can be written as:

$$\frac{\partial w}{\partial t} + \frac{\partial f}{\partial x} + \frac{\partial g}{\partial y} = \left(\frac{\partial R}{\partial x} + \frac{\partial S}{\partial y}\right) \qquad (1)$$

where w, f, g, R and S are respectively the vector unknown, the convective flux vector in x and y direction and the viscous flux vector in x and y and they are given by:

$$w = \begin{bmatrix} \rho \\ \rho u \\ \rho v \\ \rho E \end{bmatrix} \qquad f = \begin{bmatrix} \rho u \\ \rho u^2+p \\ \rho uv \\ \rho uE+up \end{bmatrix} \qquad g = \begin{bmatrix} \rho v \\ \rho vu \\ \rho v^2+p \\ \rho vE+vp \end{bmatrix}$$

$$R = \begin{bmatrix} 0 \\ \sigma_{xx} \\ \sigma_{xy} \\ u\sigma_{xx}+v\sigma_{xy}-q_x \end{bmatrix} ; \qquad S = \begin{bmatrix} 0 \\ \sigma_{xy} \\ \sigma_{yy} \\ u\sigma_{xy}+v\sigma_{yy}-q_y \end{bmatrix}$$

Where:

$$\sigma_{xx} = 2\mu u_x - \frac{2}{3}\mu(u_x+v_y)$$

$$\sigma_{yy} = 2\mu v_y - \frac{2}{3}\mu(u_x+v_y)$$

$$\sigma_{xy} = \sigma_{yx} = \mu(u_y+v_x).$$

$$q_x = -k\frac{\partial T}{\partial x}$$

$$q_y = -k\frac{\partial T}{\partial y} \quad .$$

The pressure p is obtained from the equation of state

$$P = (\gamma-1)\rho[E - \frac{1}{2}(u^2+v^2)] \quad .$$

Turbulence Model

In order to simulate turbulent flows the original version of the Baldwin Lomax [8] turbulence model has been employed in the present study.

Under the assumption of such a model the Reynold's averaged equations governing the motion of the mean flow maintains the same form of eq. (1). The coefficients of transport however must be modified as:

$$\mu = \mu_\ell + \mu_t$$

$$k = c_p\left(\frac{\mu_\ell}{Pr_\ell} + \frac{\mu_t}{Pr_t}\right)$$

to account for turbulent mixing.

3. Semidiscrete Finite Volume Formulation

(a) Cell Centered Scheme

The computational domain is divided into arbitrary quadrilateral cells. A system of ordinary differential equations is obtained by discretizing the conservation equations in integral form for the computational cell. The resulting equations have the form:

$$\frac{d}{dt}(S_{ij}\, w_{ij}) = -\, C\, w_{ij} + Dw_{ij} + ADw_{ij} \qquad (2.a)$$

where S_{ij} is the cell area. Cw_{ij} and Dw_{ij} denote respectively, the net contribution due to convection and diffusion. ADw_{ij} represents higher order adaptive dissipation terms added to prevent nonlinear instability.

The net convection flux out of the cell is computed by first evaluating the flux velocity on the k-th edge

$$Q_k = \frac{\Delta y_k\,(\rho u)_k - \Delta x_k(\rho v)_k}{\rho_k}$$

then the flux for the x momentum component, for example, is

$$C(\rho u)_{ij} = \sum_1^4{}_k [Q_k\,(\rho u)_k + \Delta y_k\, P_k]$$

where Δx_k and Δy_k are the increments of x and y along the edges with appropriate signs, and the sum is over the four sides of the computational cell. This discretization reduces to central differencing on a cartesion grid and is second order accurate on a smooth mesh.

The Gauss theorem is applied, on the path joining the centers of two adjacent cells with the end points of their dividing side, to evaluate the shear stress (σ) and heat flux (q) components at the edges of the computational cell. For example, to compute the derivatives of a generic function f(x,y) one has

$$\int_S f_x\, dS = \int_{\partial S} f(x,y)\, dy.$$

$$-\int_S f_y\, dS = \int_{\partial S} f(x,y)\, dx$$

where S is a fixed area with boundary ∂S. Then approximating the RHS integrals by trapezoidal rule yields

$$(f_x)_{i,j}\, S_{ij} = +\frac{1}{2}\left\{\sum_1^4{}_k (f_{k+1}+f_k)(y_{k+1}-y_k)\right\} ;$$

$$y_5 = y_1 \qquad f_5 = f_1$$

$$(f_y)_{i,j}\, S_{ij} = -\frac{1}{2}\left\{\sum_1^4{}_k (f_{k+1}+f_k)(x_{k+1}-x_k)\right\} ;$$

$$x_5 = x_1 \qquad f_5 = f_1 \quad .$$

The net viscous flux out of the cell for the x momentum component is

$$D(\rho u)_{ij} = \sum_{1}^{4}{}_{k}(\sigma_{xx}\,\Delta y_k - \sigma_{xy}\,\Delta x_k).$$

Where the sum is, again, on the sides of the cell.

(b) Corner Point Scheme

In this formulation the unknown variables are defined at the corners, and the system of ordinary differential equations is obtained by discretizing the conservation equations for a subdomain around each node. The resulting equations have the form:

$$\frac{d}{dt}\,(S_{ij}\,w_{ij}) = -\,C\,w_{ij} + S_{ij}\,Dw_{ij} + ADw_{ij}\,. \qquad (2.b)$$

Here S_{ij} is the sum of the areas of the four cells surrounding the node ij. Cw_{ij}, Dw_{ij}, and Aw_{ij} denote the same terms as in eq. (2.a). If one recalls that a corner point is the center of four surrounding cells, then the net convective contribution at each node is obtained as the sum of the net convective contributions over the four surrounding cells. Such a procedure guarantees conservation, is computationally efficient and yields second order accuracy on a smooth grid.

The Gauss theorem is applied twice to obtain a numerical approximation to the stress tensor (σ) and heat flux (q) at the cell centers, and their divergence directly at the nodes. The net contribution for the x-momentum component, for example, is:

$$D(\rho u)_{ij} =$$

$$\{[(\sigma_{xx_{c1}} - \sigma_{xx_{c3}})(y_{c2} - y_{c4}) - (\sigma_{xx_{c2}} - \sigma_{xx_{c4}})(y_{c1} - y_{c3})] +$$

$$- [(\sigma_{xy_{c1}} - \sigma_{xy_{c3}})(x_{c2} - x_{c4}) - (\sigma_{xy_{c2}} - \sigma_{xy_{c4}})(x_{c1} - x_{c3})]\}/$$

$$[(x_{c1} - x_{c3})(y_{c2} - y_{c4}) - (y_{c1} - y_{c3})(x_{c2} - x_{c4})]$$

Here, the subscripts c_1, c_2, c_3, c_4 denote the four centers of the cells surrounding the node ij.

4. Adaptive Dissipation

The finite volume scheme defined by equation (2.a, 2.b) is intrinsically dissipative and in principle oscillations with alternate sign at odd and even mesh points should not arise. However to guarantee that spurious oscillations do not indeed arise, some adaptive dissipation is still added to the scheme. The idea of the adaptive scheme is to add third order dissipative terms throughout the domain to provide a base level of dissipation sufficient to prevent nonlinear instability, but not sufficient to prevent oscillations in the neighborhood of shock waves. In order to capture shock waves additional first order dissipative terms are added locally by sensor designed to detect discontinuities [3].

In the solution of the Navier Stokes equations the amount of adaptive dissipation added should be reduced as much as possible in order to avoid spurious viscous-like effects. In the present study this has been achieved by appropriate scaling of the adaptive dissipation fluxes in the streamwise and normal directions. Moreover the relative size of the artificial terms has been carefully monitored. Typically for the computations of laminar flows the total value of the artificial dissipation was 10^{-3} times smaller than the physical dissipation.

5. Boundary Conditions

The existence and uniqueness of the solution of the compressible Navier-Stokes equations as a function of the boundary conditions has not been extensively investigated. In general the problem is approached in a heuristic way.

In numerical solutions it seems that a cell centered formulation is best suited for Neumann boundary conditions at solid walls, whereas the corner point discretization appears more suitable for Dirichlet boundary conditions. In the present work, at solid boundaries, the following conditions are imposed. For the cell centered scheme we require:

$$u = v = 0$$

$$\underline{n} \cdot \nabla T = 0\,.$$

For the corner point formulation we set:

$$u = v = 0$$

$$T = T_w$$

where T_w represents a given wall temperature. At the far field non-reflecting boundary conditions based on the introduction of Riemann invariants for a one dimensional flow normal to the boundary are employed.

6. Time Stepping

A three stage time stepping scheme is used for integrating equations (2.a, 2.b) in time. For economy, the diffusion terms and the dissipation operator are evaluated only at the first stage. The solution is therefore advanced from time level n to n+1 as:

$$w^{(0)} = w^{n}$$

$$w^{(1)} = w^{(0)} - \alpha_1 \left(\frac{\Delta t}{S}\right)[Cw^{(0)} - Dw^{(0)} - ADw^{(0)}]$$

$$w^{(2)} = w^{(0)} - \alpha_2 \left(\frac{\Delta t}{S}\right)[Cw^{(1)} - Dw^{(0)} - ADw^{(0)}]$$

$$w^{(3)} = w^{(0)} - \alpha_3 \left(\frac{\Delta t}{S}\right)[Cw^{(2)} - Dw^{(0)} - ADw^{(0)}]$$

$$w^{n+1} = w^{(3)}$$

Where the coefficients are given by:

$$\alpha_1 = \alpha_2 = .6 \qquad \alpha_3 = 1.$$

7. Convergence Acceleration

Acceleration of convergence to steady state has been achieved by the following means:

i) At each computational cell the solution is advanced in time at its own Δt limit so as to propagate any disturbance out of the field at a rate proporational to the number of points in the outward direction.

ii) Use of implicit smoothing of the residuals to increase the stability region of the multistage scheme, yielding a higher permissible CFL number [3].

iii) The multigrid strategy devised by Jameson [3] for the solution of the Euler equations has been extended for the Navier Stokes equations. Auxiliary meshes are introduced by doubling the mesh spacing. Values of the flow variables are transferred to a coarser grid by a rule that conserves mass, momentum and energy. The multistage scheme is reformulated as described in Ref. [3] with the result that the solution on a coarse grid is driven by the residuals collected on the next finer grid. The process is repeated on successively coarser grids. Finally the corrections are passed back to the next finer grid by bilinear interpolation. An effective multigrid strategy is to use a simple sawtootch cycle, in which a transfer is made from each grid to the next coarser grid after a single time step. After reaching the coarser grid, the corrections are then interpolated back from each grid to the next finer grid without any intermediate Navier-Stokes computation.

Results

Both corner point and cell centered schemes have been tested for the solution of laminar flow problems. Detailed results of external [9] as well as internal [10] flows have been reported elsewhere. In the next sections we present some applications to laminar and turbulent flows over simple airfoils.

Laminar Flows on an NACA 0012 Airfoil

Results of subcritical, transonic and supersonic flows on a NACA 0012 airfoil computed with the corner point scheme are discussed first.

(a) Subsonic laminar flow
($M_\infty = .5$, $Re_\infty = 5{,}000$, $\alpha = 0^\circ$).

The effectiveness of the multigrid algorithm in accelerating the convergence to steady state is shown by this first set of results. In a recent study. Swanson and Turkel [5] reported results for the flow field on a NACA 0012 airfoil at $M_\infty = .5$, $Re_\infty = 5{,}000$ and 0° angle of attack. They were using a multistage cell centered formulation together with enthalpy damping to achieve convergence. They found that approximatively 1,300 cycles were necessary to converge within engineering precision. We run the corner point scheme on a 192x48 C-mesh with 5/8 of the total number of points placed on the airfoil (Figure 1). The computed surface pressure distribution (Figure 2) is in close agreement with the one reported in Ref [5]. Convergence history for this case (Figure 3) is quite satisfactory and the steady state is reached within 300 multigrid cycles.

(b) Transonic Laminar Flow
($M_\infty = .8$, $Re_\infty = 500$, $\alpha = 10^\circ$).

The solution for this case was computed on a 256 x 64 C-mesh (Figure 4) obtained by using an hyperbolic grid generation technique. Again 5/8 of the points in the streamwise direction were placed on the airfoil. The flow field boundary was located 18 chords away from the airfoil and the first point in the boundary layer was located at .002 chords away from the wall. That this case is particularly difficult is immediately evident from the computed results (Figures 5-6). Significant viscous effects are present everywhere on the airfoil. On the leading edge the suction region is moved away from the airfoil. Mildly supersonic conditions are however achieved on the top surface and the flow is turned back to subsonic through the edge of the boundary layer. After laminar separation occurs, a large recirculation region is formed downstream on the top surface. In this region the velocities are extremely small and accuracy is of special concern. However coarse (128x32) and fine mesh computations of the extent of the separated region and the location of the separation point agree closely, indicating that these flow characteristics are reasonably well predicted.

The results presented were obtained after 300 cycles of the multigrid on a scalar machine (IBM 3081). Further computations performed on a CRAY XMP show that indeed steady state solution is established in approximately 300 cycles and that convergence history continues to exhibit a monotone behavior up to 1,200 cycles (Figure 7).

(c) Supersonic Laminar Flow
($M_\infty = 2$, $Re_\infty = 106$, $\alpha = 10^\circ$).

Computations of this supersonic lifting flow were performed on the same mesh described in (b). The choice of this case was motivated by the availability of experimental data [11]. A comparison between measured and computed iso-density lines is shown in Figure 8. The agreement is fairly good, especially near the leading edge. The location of the bow shock wave is also well predicted. Discrepancies near the trailing edge are most probably produced by the boundary conditions. In the computations adherence conditions are strictly enforced whereas the measurements, which were made with a rarefied gas, suggest that slip velocities were present on the airfoil.

Turbulent flows on a RAE 2822 Airfoil

In this section we present solutions to the Reynold's averaged equations for the follow ng test cases:

(i) $\alpha = 1.93$ $M_\infty = .676$ $Re_\infty = 5.7\ 10^6$
(ii) $\alpha = 2.79$ $M_\infty = .73$ $Re_\infty = 6.5\ 10^6$

For these computations we used a 256 x 64 C-mesh similar to the one already described. However the height of the first cell was reduced to 2×10^{-5} chords in order to provide the clustering of points needed to resolve the thin boundary layer characteristic of high Reynold's number flows. The cell aspect ratio for this grid is therefore very high (up to 1,000) (Figure 9).

As in the case of laminar flows we found that 300 cycles of the multigrid are sufficient to reach a steady state solution. A typical convergence history for the C_L is shown in Figure 10. However a noticeable slowdown in the convergence rate measured by the averaged residuals was also observed.

For case (i) a comparison of the computed surface pressure and skin friction shows very good agreement between the results obtained from the cell centered scheme (Figures 11-12) and the corner point scheme (Figures 13-14). This is also verified by the comparison of the computed aerodynamic coefficients as summarized in Table 1, where computed results obtained from the ARC2D program [6] are also reported together with the experimental values [12].

The results for case (ii) verify the good shock capturing properties of the scheme (Figure 15). Again, for this case, the computations are in reasonable agreement with the results from ARC2D (Table 2). An interesting common feature of our results and those reported by Pulliam [6] is the prediction of small regions of separation at the foot of the shock and at the upper trailing edge (Figure 16) not present in the experiments. However, the shock locations and strength compare very well with the measurements.

9. Conclusions

An explicit multistage algorithm for the solution of the Navier Stokes equations has been developed and applied to both corner point and cell centered formulations. It has been shown that computational efficiency is enhanced by using a multigrid technique. The computed solutions of laminar flows show qualitative and quantitative agreement with experiments and/or other computations. The convergence history for laminar computations was found to be satisfactory.

The scheme has also been successfully applied to the Reynold's averaged equations. The computed results were found to be in close agreement with other computations. The marked slowdown in the convergence rate observed for all the turbulent computations suggests that a rigorous study on the effects of high aspect ratio cell is needed. Planned extensions of this work include implementation of a two equation turbulence model and use of a grid embedding technique to increase the resolution within the boundary layer.

Acknowledgement

The authors wish to thank the Boeing Company for providing access to its computational facilities. We are also indebted to L. Wigton of the Boeing Commercial Aircraft Company for providing us with his hyperbolic grid generation code.

References

1. Jameson, A., Schmidt, W. and Turkel, E., "Numerical Solutions of the Euler Equations by Finite Volume Methods using Runga-Kutta Time-Stepping Schemes", AIAA Paper 81-1259, June 1981.

2. Jameson, A., Baker, T. and Weatherill, N., "Calculation of the Inviscid Transonic Flow Over a Complete Aircraft", AIAA Paper 86-0103, January 1986.

3. Jameson, A., "Transonic Flow Calculations", MAE Report #1651, Princeton University, July 1983.

4. Agarwal, R. and Deese, J., "Computation of Transonic Viscous Airfoil, Inlet and Wing Flowfields", AIAA Paper 84-1551, June 1984.

5. Swanson, R.C., Turkel, E., "A Multistage Time-Stepping Scheme for the Navier Stokes Equations", AIAA Paper No. 85-0035, January 1985.

6. Pulliam, T., "Euler and Thin Layer Navier Stokes Codes: ARC2D, ARC3D", Notes for Computational Fluid Dynamics User's Workshop, March 1984.

7. Barth, T., Pulliam, T. and Buning, P., "Navier Stokes Computations for Exotic Airfoils", AIAA Paper 85-0109, January 1985.

8. Baldwin, B.S. and Lomax, H., "Thin Layer Approximation and Algebraic Model for Separated Turbulent Flows", AIAA Paper 78-257, January 1978.

9. Jameson, A., Martinelli, L., Grasso, F., "A Multistage Multigrid Method for the Navier Stokes Equations", GAMM Workshop on Numerical Simulation of Compressible Navier-Stokes Flows, Sophia Antipolis, December 4-5, 1985.

10. Bassi, F., Grasso, F., Jameson, A., Martinelli, L. and Savini, M., "Single Grid Solution of the Compressible Navier Stokes Equations on a H-Mesh", GAMM Workshop on Numerical Simulation of Compressible Navier-Stokes Flows, Sophia Antipolis, December 4-5, 1985.

11. Allegre, J., Lengrand, J.C. and Raffin, M., "Champs D'Ecoulement Rarefies Compressibles Autour D'Un Profil NACA 0012", Rapport Sessia 894/82.380, November 1982.

12. Cook, P., McDonald, M. and Firmin, M.C.P., "Aerofoil RAE 2822 - Pressure Distributions, and Boundary layer and Wake Measurements", AGARD-AR-138, 1979.

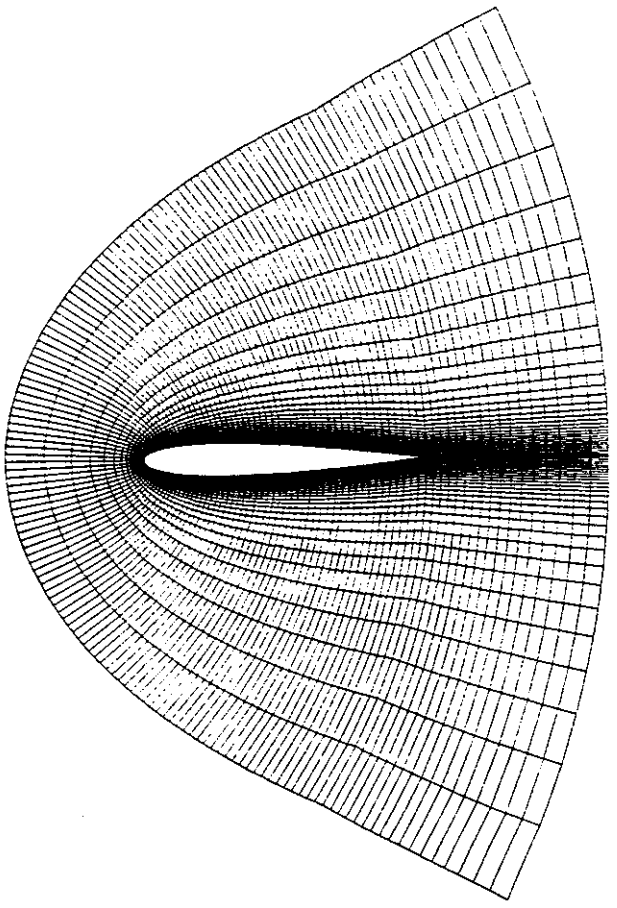

Figure 1.
Partial view of the grid for laminar calculation.
case (a)

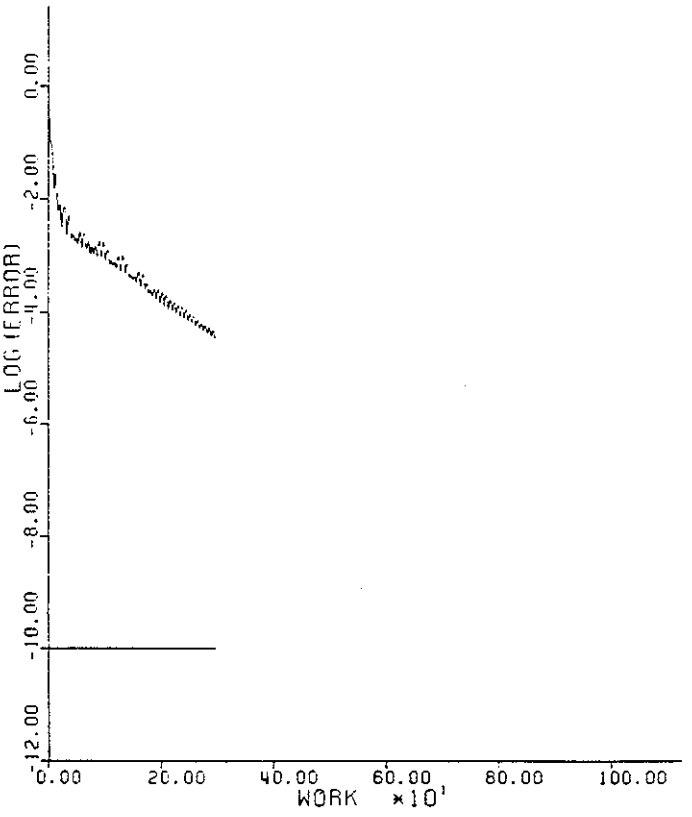

Figure 3.
Convergence history as measured by the RMS value
of density residual for case (a).

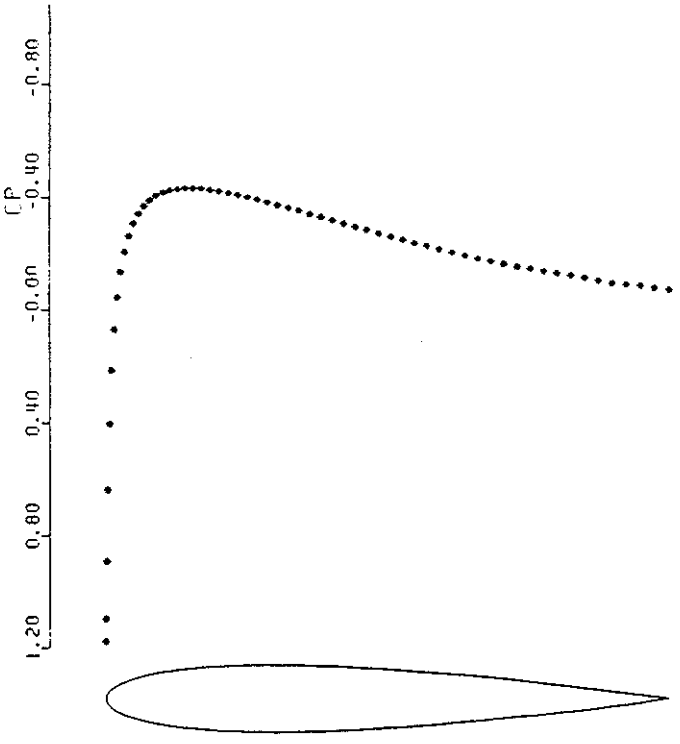

Figure 2.
Pressure distribution for subcritical laminar flow,
case (a)

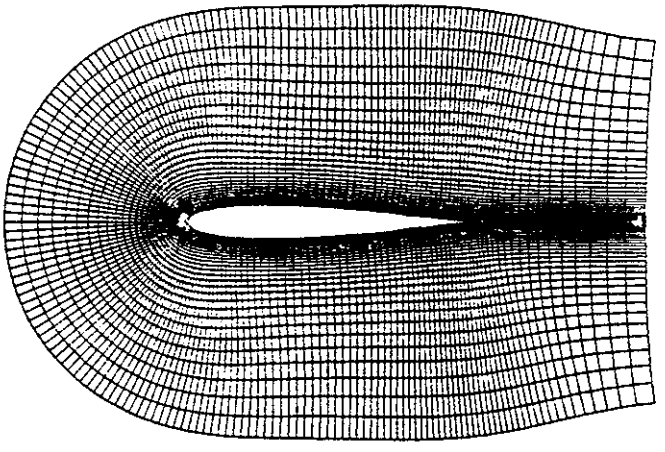

Figure 4.
Partial view of the grid for laminar calculations.
cases (b) and (c).

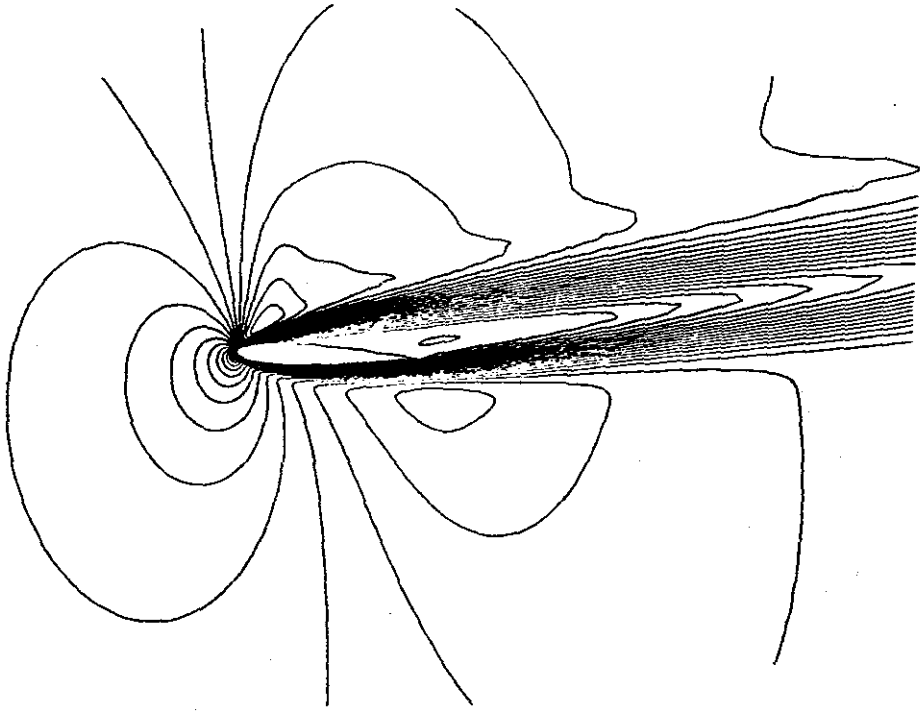

Figure 5.
Iso-Mach contours for transonic laminar flow.
case (b)

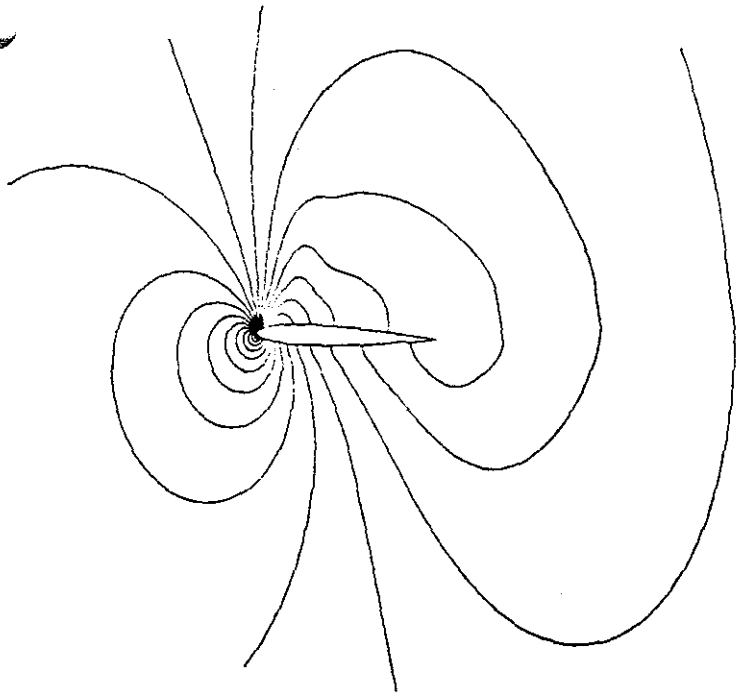

Figure 6.
Iso-Pressure contours for transonic laminar flow.
case (b)

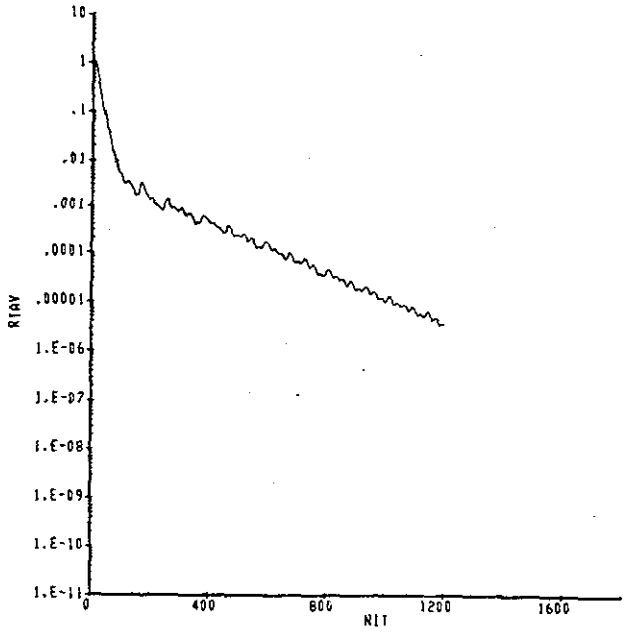

Figure 7.
Convergence history as measured by the RMS value
of density residual for case(b).

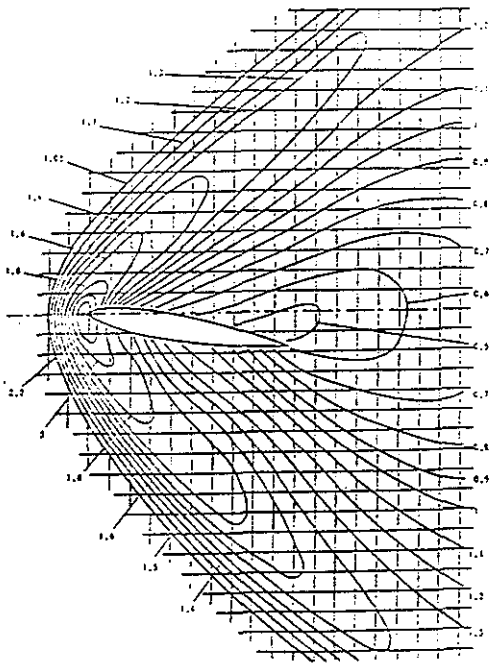

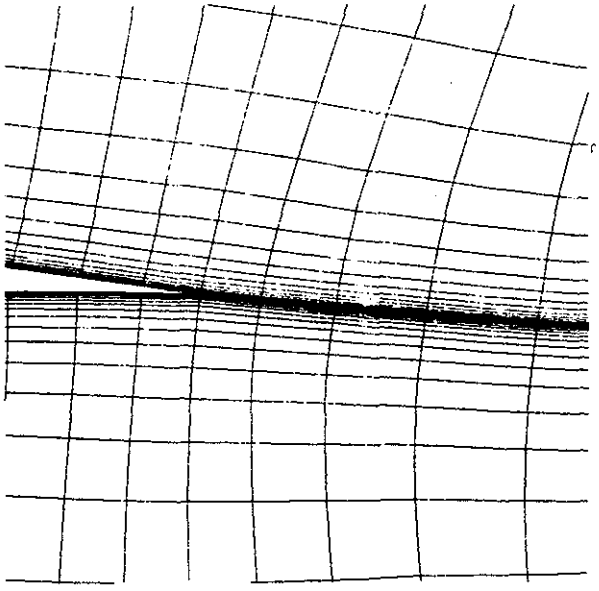

Figure 9.
Blowup of the trailing edge region for a typical mesh for high Reynolds number flows.

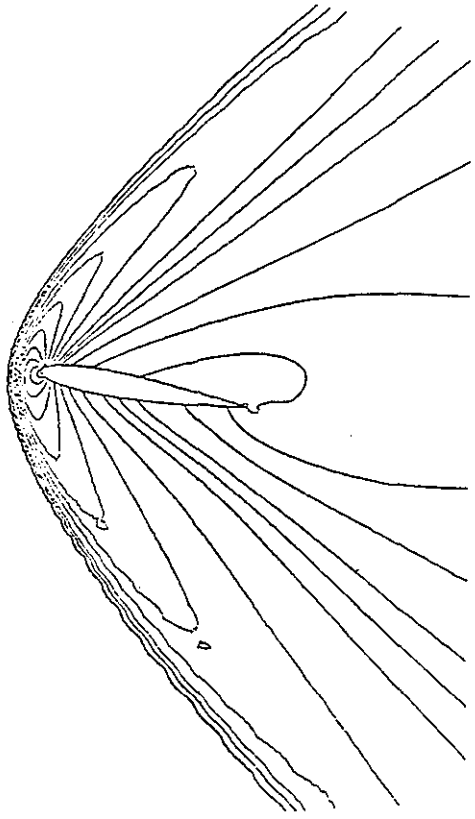

Figure 8.
Comparison of measured [11] and computed isodensity line for supersonic laminar flow. case (c)

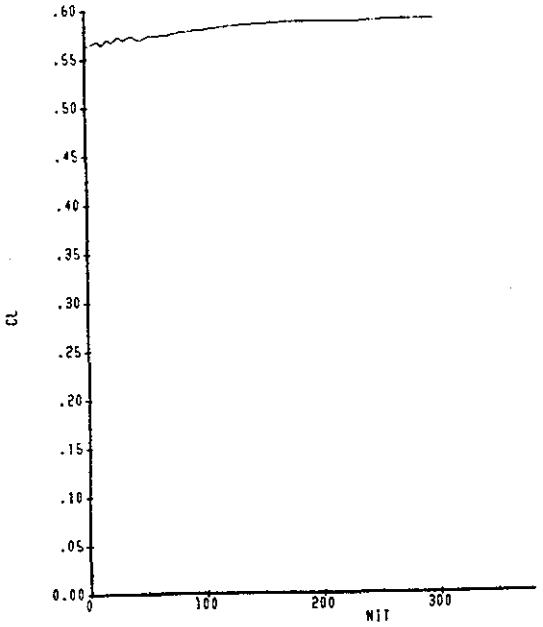

Figure 10.
Typical convergence history measured by lift coefficient C_L.

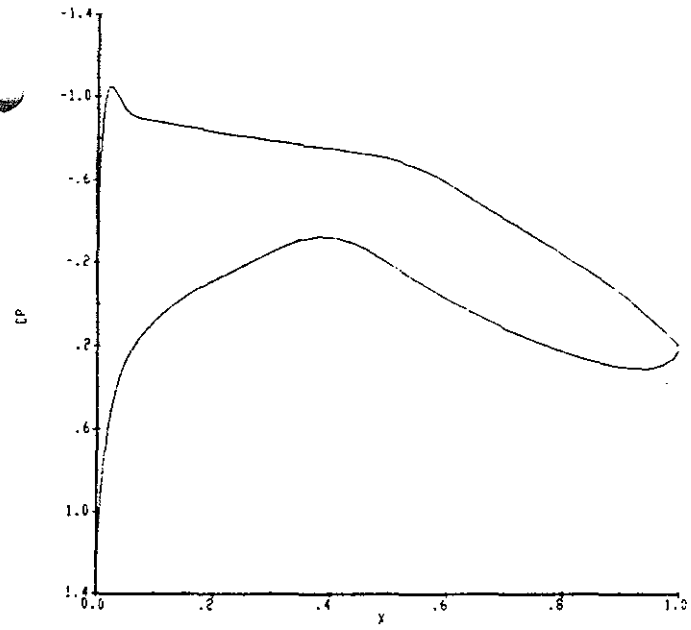

Figure 11.
Pressure distribution - cell centered scheme.
case (i)

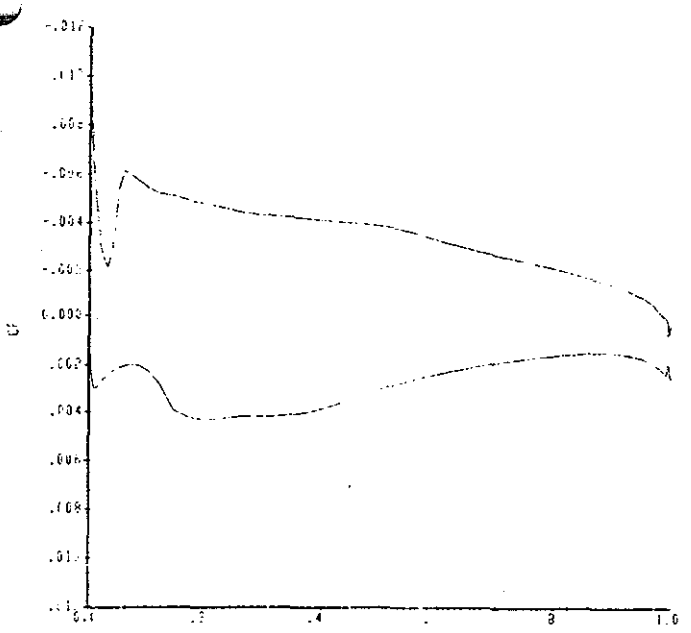

Figure 12.
Skin friction - cell center scheme.
case (i)

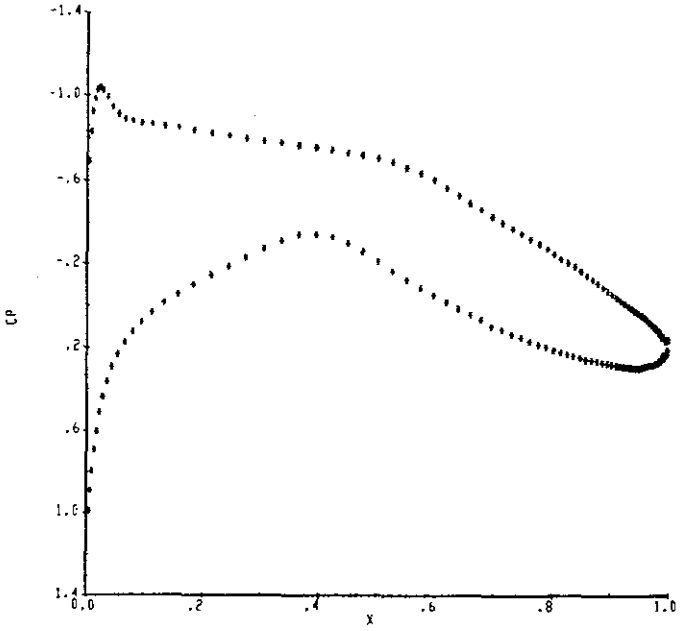

Figure 13.
Pressure distribution - corner point scheme.
case (i)

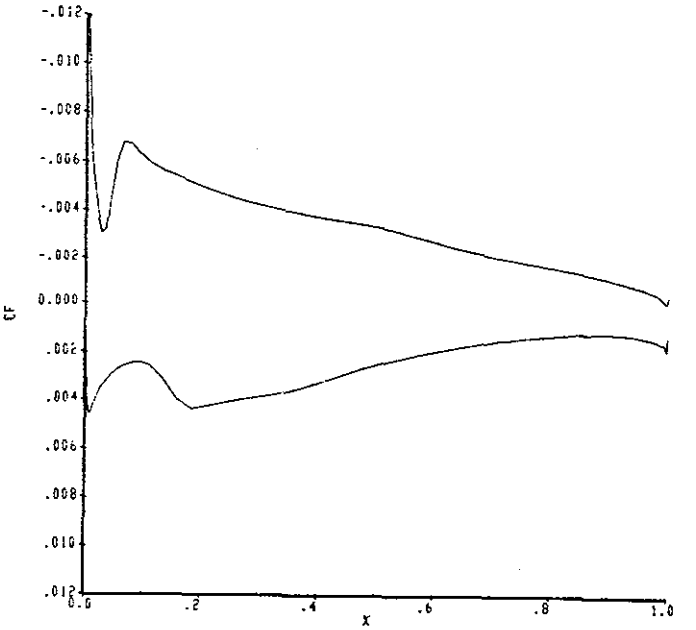

Figure 14.
Skin friction - corner point scheme.
case (i)

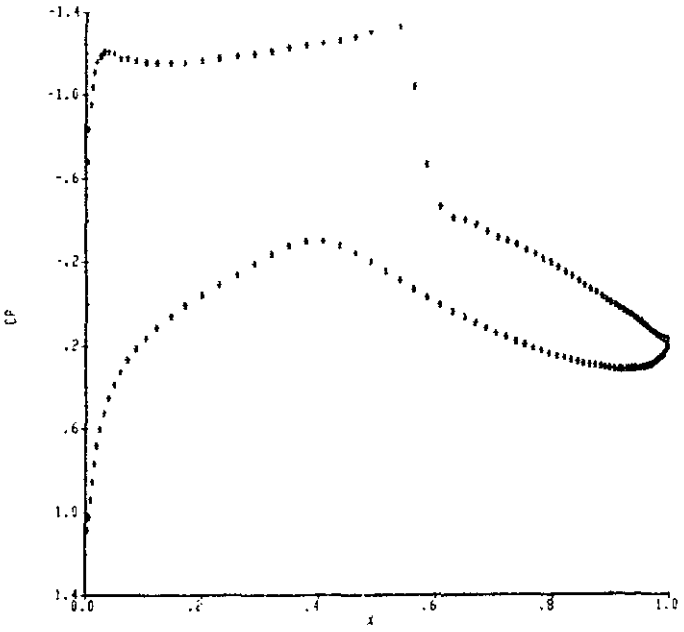

Figure 15.
Pressure distribution - cell centered scheme.
case (ii)

RAE 2822	M = .6?6	Re_∞ = 5.7 x 10^6		α = 1.93°
	C_L	C_D (Pressure)	C_M	Grid
Experiments (Ref. 12)	.566	-	-.082	-
Cell Centered	.588	.030	-.083	256x64 C-Mesh
Corner Point	.579	.040	-.084	256x64 C-Mesh
ARC2D Code	.596	.047	-.088	256x64 C-Mesh
Pulliam 1984 (Ref. 6)	.587	.038	-.084	251x51 O-Mesh

Table 1.

Measured and computed force coefficients.
Case (i)

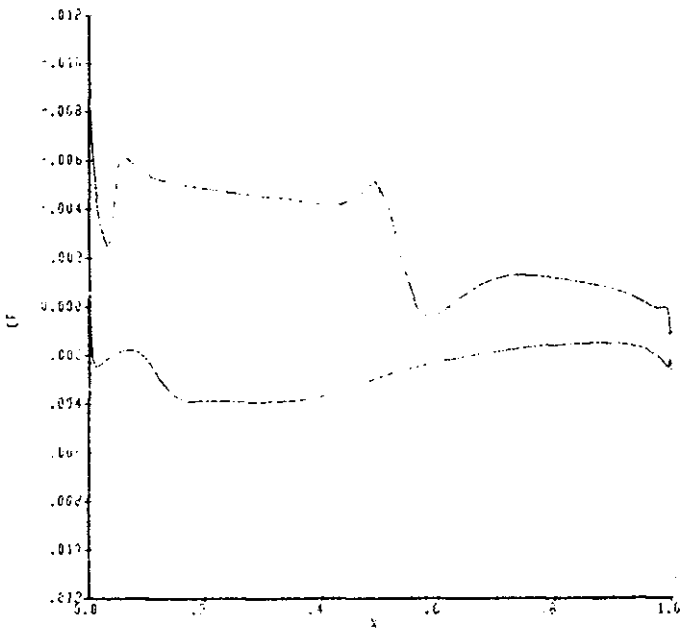

Figure 16.
Skin friction - cell centered scheme.
case (ii)

RAE 2822	M = .73	Re_∞ = 6.5 x 106		α = 2.79o
	C_L	C_D (Pressure)	C_M	Grid
Experiments (Ref. 12)	.803	-	-.099	-
Cell Centered	.835	.0122	-.096	256x64 C-Mesh
ARC2D Code	.839	.0118	-.096	256x64 C-Mesh
Pulliam 1984 (Ref. 6)	.825	.0123	-.095	251x51 O-Mesh

Table 2.

Measured and computed force coefficients.
Case (ii)